Acta Mech 229, 437–454 (2018)
https://doi.org/10.1007/s00707-017-1980-7

ORIGINAL PAPER

Alberto Di Matteo · Thomas Furtmüller · Christoph Adam · Antonina Pirrotta

Optimal design of tuned liquid column dampers for seismic response control of base-isolated structures

This paper is dedicated to the memory of Franz Ziegler

Received: 17 October 2016 / Revised: 17 March 2017 / Published online: 15 November 2017

Abstract In this paper, the use of a tuned liquid column damper (TLCD) as a cost-effective means to control the seismic response of a base-isolated structure is studied. A straightforward direct approach for the optimal design of such a device is proposed, considering a white noise model of the base excitation. On this base, a direct optimization procedure of the TLCD design parameters is performed and optimal design charts are presented as a ready-to-use practical design tool. Comparison with the optimal parameters obtained considering a classical iterative statistical linearization technique proves the reliability of the proposed approach. The performance of the base-isolated TLCD-controlled structure is examined and compared with that of the simple base-isolated one (without TLCD), using a set of 44 recorded ground motions as base excitation. Theoretical and numerical results show that the TLCD is rather effective in reducing the response of base-isolated structures under strong earthquakes. Therefore, considering its advantageous characteristics and its overall beneficial effects, TLCDs can be considered as practical and appealing means to control the seismic response of base-isolated structures.

1 Introduction

Seismic base-isolation is one of the most effective and widely used means for protection of relatively stiff structures against earthquake excitation. Through a base-isolation subsystem, the structure is virtually decoupled from the ground. Decoupling is achieved by inserting a layer of low horizontal and high vertical stiffness between the structure and its foundation, shifting the fundamental natural frequency of the entire structural system away from the range of frequencies that dominate the earthquake excitation [16]. In this manner, the structure on the base-isolation system tends to behave like a rigid body, since the majority of the displacement

A. Di Matteo · A. Pirrotta
Dipartimento di Ingegneria Civile, Ambientale, Aerospaziale, dei Materiali (DICAM), Università degli Studi di Palermo, 90128 Palermo, Italy
E-mail: alberto.dimatteo@unipa.it

T. Furtmüller · C. Adam (✉)
Unit of Applied Mechanics, University of Innsbruck, 6020 Innsbruck, Austria
E-mail: christoph.adam@uibk.ac.at

T. Furtmüller
E-mail: thomas.furtmueller@uibk.ac.at

A. Pirrotta
Department of Mathematical Sciences, University of Liverpool, Liverpool, UK
E-mail: antonina.pirrotta@unipa.it

occurs within the base-isolation system itself. Hence, structure displacements and accelerations are greatly reduced, while the base-isolation subsystem undergoes large, and sometimes undesirable, displacements.

Several research efforts have been focused on the reduction in this displacement demand of the base-isolation subsystem, resorting to many different strategies. One common way, for instance, consists in providing supplemental damping to the isolation layer, which, however, may lead to an increase in the interstory drifts and accelerations of the main structure [17].

In this context, some researchers began to consider using passive vibration control devices, such as the well-known tuned mass damper (TMD), to improve the performance of base-isolation systems. Specifically, initial studies can be found in [33] and [29], where the effect of the TMD on base-isolated structures and the choice of the proper TMD parameters have been investigated. Further, in [22] it has been demonstrated that the TMD is more effective at reducing the structural response for low damping in the base-isolation subsystem, and in general TMDs can lead to better control performance than providing supplemental damping to the isolation layer [21], since small interstory drifts typical of base-isolated structures are preserved, while the displacement demand of the base-isolation subsystem is reduced [2]. As far as the optimal choice of the TMD parameters attached to base-isolation subsystems is concerned, some analyses in the frequency domain are presented in [33], while in [27] optimal TMD design parameters are determined considering the case of a white noise ground excitation. More recently, in [31] the optimization of a non-traditional TMD, with minor stroke length demand, is discussed. Finally it is worth noting that, apart from the case of a ground excitation, in [15] the performance of a base-isolated structure equipped with a TMD device has been studied considering a wind type of excitation, demonstrating that attaching a TMD at the roof or base can reduce the structural response significantly.

In all the previous investigations, only the case of TMD devices connected to the base-isolated structures has been analyzed. In this regard, there are very few studies in which other passive control devices have been considered for reducing the displacement demand of base-isolated structures. Specifically, in [20] the case of a tuned liquid damper (TLD) device has been examined for wind induced motion of base-isolated buildings.

One interesting control device, which in recent years has attracted the attention of an increasing number of researchers, is the so-called tuned liquid column damper (TLCD). The TLCD is a passive vibration control device that dissipates structural vibrations through the motion of a liquid column inside U-shaped containers, based on the same mechanical principle as the TMD. The liquid column can freely flow inside the U-shaped container, and the liquid surface in the two vertical columns of the container is under constant atmospheric pressure. In this manner, the natural frequency of oscillation of the liquid theoretically depends only on the total length of the liquid column [1,13], thus making TLCDs particularly suitable for systems characterized by a predominant first mode with very low fundamental natural frequency, as in the case of base-isolated structures.

To overcome the limitation of applicability to structures with very low fundamental frequencies, Ziegler and coworkers (see, e.g., [14,24,25,35]) have developed the highly innovative tuned liquid column gas damper (TLCGD), where in contrast to the TLCD both ends of the U-shaped tube are sealed, and thus, the gas-spring effect is activated [11,35], pushing the frequency range applicability of such devices up to 5 Hz [14]. Active control of pressure input into the gas volume (ATLCGD) even allows to reduce the transient structural vibration peaks, observed in the initial period of the strong motion phase of earthquakes [13,14]. Recently, several general on-off damping controller for a semi-active TLCD has been implemented [19]. In [35], Ziegler proposed a novel TLCD for mitigating vertical vibrations. Hochrainer and Ziegler [14] used for the first time a TLCD to control a base-isolated five-story generic frame structure. More recently, Khalid and Ziegler [18] studied a novel base-isolation system with effective damping supplied by a TLCGD. For a complete overview on the application of the TLCD and its passive and active variants in buildings, bridges and dams, the reader is referred to Hochrainer and Ziegler [12].

The TLCD is generally modeled as a single-degree-of-freedom (SDOF) system rigidly connected to a vibrating structure [6,8,13], and its effectiveness depends on proper tuning of the natural frequency and damping ratio, such as in a TMD. However, unlike the traditional TMD, the TLCD response is nonlinear [5,9] and the optimal damping parameters cannot be established a priori unless the forcing magnitude is known and numerical optimization methods are required (see [7] and references therein).

Due to some of their beneficial characteristics (such as low cost, easy implementation, lack of required maintenance, no need to add mass to the structure when using the liquid as water supply), TLCD represents now an attractive alternative for vibrations mitigation. Readers may refer to Ziegler [34] for a detailed analysis on the beneficial features of TLCDs among different types of passive vibration control systems.

Based on the pioneering applications of Ziegler [14,18], and in the context of taking into account these attractive characteristics, in this paper the control performance of a TLCD on the seismic response of a base-isolated structure is investigated. Once the nonlinear equations of motion of a TLCD-controlled multi-degree-of-freedom (MDOF) base-isolated structure are derived, the classical statistical linearization technique (SLT) is applied to analyze the statistics of the response in case of a Gaussian white noise ground excitation, and comparison with Monte Carlo simulation data is used to prove the reliability of the results. Since SLT requires several computationally expensive numerical iterations, a straightforward procedure is proposed that allows for the direct evaluation of the equivalent linear system parameters and corresponding steady-state response variances, under some reasonable assumptions regarding base-isolated structures. In order to prove the reliability of the proposed approach, comparison with the SLT is provided, showing a satisfactory agreement between the two approaches, even when the aforementioned assumptions are removed. Further, taking full advantages of this proposed direct evaluation of the equivalent linear system parameters, a direct optimization procedure of the TLCD design parameters is performed, aiming at maximally control the seismic response of the base-isolated structure. Optimal design charts are introduced as a ready-to-use practical design tool. Comparison with the optimal parameters obtained by a rather elaborate numerical optimization procedure, based on the classical iterative SLT, is carried out leading to very small discrepancies especially in terms of control performances. It is worth mentioning that a significant reduction in computational effort is achieved with the proposed straightforward approach. Finally, to show the influence of the non-stationary nature of real ground motions, the control performances of the TLCD device directly connected to the base-isolation subsystem are examined employing time-history analyses using the 44 recorded ground motions of the FEMA P-695 far-field (FEMA P-695-FF) set described in [10]. Specifically, a 20-story benchmark base-isolated building, used in [33], has been taken into account. It is shown that the TLCD device leads to a 16% reduction in the median of the relative peak base-isolation subsystem displacement, compared to the case of the base-isolated structure without TLCD.

2 Problem formulation

Let the equations of motion of a planar frame with lumped mass and n degrees-of-freedom (main structure) subjected to a horizontal earthquake ground acceleration $\ddot{x}_g(t)$ be given in classical matrix form as

$$\mathbf{M}\ddot{\mathbf{x}}(t) + \mathbf{C}\dot{\mathbf{x}}(t) + \mathbf{K}\mathbf{x}(t) = -\mathbf{M}\mathbf{r}\ddot{x}_g(t), \tag{1}$$

where $\mathbf{M}$, $\mathbf{C}$ and $\mathbf{K}$ are the $n \times n$ mass, damping and stiffness matrix, respectively, of the structure, $\mathbf{x}$ is the vector containing the nodal deformations of the structure, $\mathbf{r}$ is the location vector and a dot over a variable stands for derivation with respect to time t. Equation (1) can be rewritten as

$$M_i\ddot{x}_i(t) + \sum_{j=1}^{n} C_{i,j}\dot{x}_j(t) + \sum_{j=1}^{n} K_{i,j}x_j(t) = -M_i\ddot{x}_g(t) \qquad (i = 1,\ldots,n), \tag{2}$$

where the terms M_i, $C_{i,j}$ and $K_{i,j}$ in Eq. (2) correspond to the entries of the matrices $\mathbf{M}$, $\mathbf{C}$ and $\mathbf{K}$, while x_i is the ith nodal deformation of the structure relative to the ground.

Consider now the case in which the structure is separated through a base-isolation subsystem from the foundation for earthquake protection purposes, as shown in Fig. 1a for the example of a shear-type frame structure. The response of this base-isolated structure is governed by the following equations [29]:

$$\begin{aligned} M_{\text{tot}}\ddot{x}_b(t) + \sum_{i=1}^{n} M_i\ddot{x}_i(t) + C_b\dot{x}_b(t) + K_b x_b(t) &= -M_{\text{tot}}\ddot{x}_g(t), \\ M_i\ddot{x}_b(t) + M_i\ddot{x}_i(t) + \sum_{j=1}^{n} C_{i,j}\dot{x}_j(t) + \sum_{j=1}^{n} K_{i,j}x_j(t) &= -M_i\ddot{x}_g(t) \qquad (i = 1,\ldots,n), \end{aligned} \tag{3}$$

where M_b, C_b and K_b are, respectively, mass, damping and stiffness of the base-isolation subsystem (modeled as a linear system), x_b is its displacement relative to the ground and $M_{\text{tot}} = M_b + \sum_{i=1}^{n} M_i$. Here, the nodal structural deformations x_i are measured relative to x_b, compare with Fig. 1b.

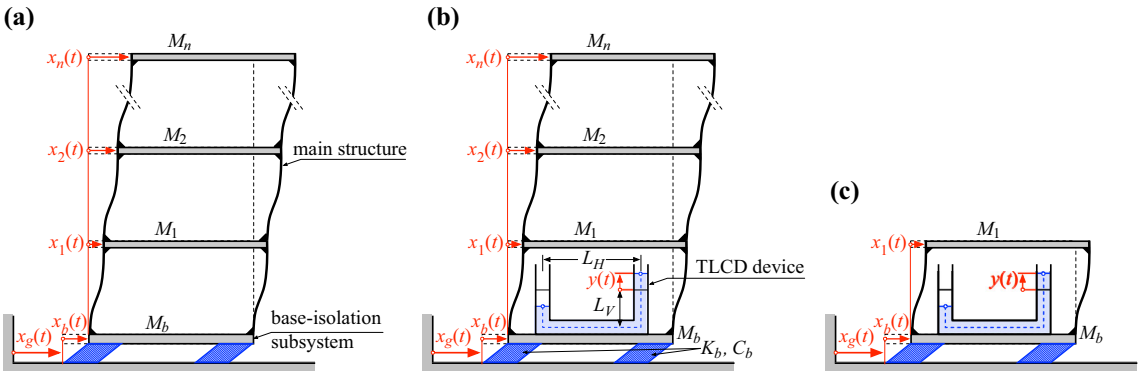

Fig. 1 Base-isolated structures: **a** MDOF shear-type frame without TLCD; **b** hybrid-controlled MDOF shear-type frame with TLCD; **c** hybrid-controlled SDOF shear frame with TLCD

When dealing with a SDOF main structure (i.e., $n = 1$), Eq. (3) reverts to

$$\begin{aligned} &\ddot{x}_b(t) + \mu_1 \ddot{x}_1(t) + 2\zeta_b \omega_b \dot{x}_b(t) + \omega_b^2 x_b(t) = -\ddot{x}_g(t), \\ &\ddot{x}_b(t) + \ddot{x}_1(t) + 2\zeta_1 \omega_1 \dot{x}_1(t) + \omega_1^2 x_1(t) = -\ddot{x}_g(t), \end{aligned} \tag{4}$$

where $\mu_1 = M_1/M_{\text{tot}}$, $\omega_b = \sqrt{K_b/M_{\text{tot}}}$ and $\zeta_b = C_b/(2M_{\text{tot}}\omega_b)$ are the natural frequency and damping ratio of the base-isolation system, respectively, while $\omega_1 = \sqrt{K_1/M_1}$ and $\zeta_1 = C_1/(2M_1\omega_1)$ are the natural frequency and damping ratio of the SDOF main structure.

Aiming at reducing the displacement demand x_b of the isolation subsystem, consider now the case of the above-described base-isolated multi-story structure in which a TLCD device with constant tubular cross section is rigidly attached to the base plate of the base-isolation subsystem, as shown in Fig. 1b. Denoting with g the gravitational acceleration, L_v and L_h the vertical and horizontal liquid length, respectively, $L = L_h + 2L_v$ the total length of the liquid inside the TLCD, the corresponding equations of motion of this $n + 2$ degrees-of-freedom system can be written as

$$\begin{aligned} &(M_{\text{tot}} + m_l)\ddot{x}_b(t) + m_h\ddot{y} + \sum_{i=1}^{n} M_i \ddot{x}_i(t) + C_b\dot{x}_b(t) + K_b x_b(t) = -(M_{\text{tot}} + m_l)\ddot{x}_g(t), \\ &m_h\ddot{x}_b(t) + m_l\ddot{y}(t) + \frac{m_l}{2L}\xi|\dot{y}(t)|\dot{y}(t) + 2\frac{m_l}{L}g\,y(t) = -m_h\ddot{x}_g(t), \\ &M_i\ddot{x}_b(t) + M_i\ddot{x}_i(t) + \sum_{j=1}^{n} C_{i,j}\dot{x}_j(t) + \sum_{j=1}^{n} K_{i,j}x_j(t) = -M_i\ddot{x}_g(t) \qquad (i = 1, \ldots, n), \end{aligned} \tag{5}$$

where m_l is the total liquid mass inside the TLCD device, $m_h = \alpha m_l$ is the horizontal liquid mass, being $\alpha = L_h/L$ the so-called length ratio, $y(t)$ is the displacement of the liquid surface and ξ is the head loss coefficient. Note that Eq. (5) represents a set of $n + 2$ differential equations, the second of which is nonlinear. Specifically, the nonlinear term is generally used to model head losses caused by the presence of an orifice inside the TLCD and viscous interaction between the liquid and rigid container wall [6].

For an SDOF main structure ($n = 1$) as depicted in Fig. 1c, the equations of motion (5) are particularized as

$$\begin{aligned} &(1 + \mu_l)\ddot{x}_b(t) + \alpha\mu_l\ddot{y} + \mu_1\ddot{x}_1(t) + 2\zeta_b\omega_b\dot{x}_b(t) + \omega_b^2 x_b(t) = -(1 + \mu_l)\ddot{x}_g(t), \\ &\alpha\ddot{x}_b(t) + \ddot{y}(t) + \frac{1}{2L}\xi|\dot{y}(t)|\dot{y}(t) + \omega_l^2 y(t) = -\alpha\ddot{x}_g(t), \\ &\ddot{x}_b(t) + \ddot{x}_1(t) + 2\zeta_1\omega_1\dot{x}_1(t) + \omega_1^2 x_1(t) = -\ddot{x}_g(t), \end{aligned} \tag{6}$$

where $\mu_l = m_l/M_{\text{tot}}$ is the liquid mass ratio and $\omega_l = \sqrt{2g/L}$ is the natural frequency of oscillation of the liquid column inside the TLCD [13]. Since the damping term in Eq. (6b) is nonlinear, even assuming that the base-isolation subsystem and the main structure behave linearly, the whole system experiences inherent nonlinear properties. Therefore, some difficulties may arise for the optimal design of the damper device in order to obtain the maximum reduction in the displacement demand of the isolation subsystem.

In the following section, a procedure based on statistical linearization will be introduced to overcome these difficulties.

2.1 Statistical linearization of base-isolated structure equipped with TLCD

Suppose that the latter base-isolated SDOF structure equipped with a TLCD (Fig. 1c) is driven by random base excitation, such as earthquake ground accelerations, that can be modeled as a zero-mean Gaussian white noise process. It follows that the displacements of the liquid column and the base-isolation subsystem, nodal structural deformations and their derivatives are stochastic processes too (denoted by capital letters, as customary). Moreover, due to the presence of the nonlinear damping term, responses are non-Gaussian processes.

However, taking full advantage of the powerful tool of the Statistical Linearization Technique (SLT), the original nonlinear system (6) can be replaced by a linear equivalent one as

$$\begin{aligned}(1+\mu_l)\,\ddot{X}_b(t)+\alpha\mu_l\ddot{Y}+\mu_1\ddot{X}_1(t)+2\zeta_b\omega_b\dot{X}_b(t)+\omega_b^2X_b(t)&=-(1+\mu_l)\,\ddot{X}_g(t)\,,\\ \alpha\ddot{X}_b(t)+\ddot{Y}(t)+2\zeta_l\omega_l\dot{Y}(t)+\omega_l^2Y(t)&=-\alpha\ddot{X}_g(t)\,,\\ \ddot{X}_b(t)+\ddot{X}_1(t)+2\zeta_1\omega_1\dot{X}_1(t)+\omega_1^2X_1(t)&=-\ddot{X}_g(t)\,,\end{aligned}\tag{7}$$

where ζ_l is the equivalent damping ratio of the TLCD, obtained by minimizing the mean square with respect to ξ. Specifically, following the analysis in [4,26], the expression for the equivalent damping ratio becomes

$$\zeta_l=\frac{\xi}{2L\,\omega_l}\sqrt{\frac{2}{\pi}}\sigma_{\dot{Y}},\tag{8}$$

where $\sigma_{\dot{Y}}$ is the standard deviation of the velocity of the liquid column. As shown in [4], the application of Eq. (8) for design purposes is not straightforward since $\sigma_{\dot{Y}}$ is still unknown and implicitly depends on the equivalent damping ratio ζ_l. Therefore, generally an iterative procedure is necessary. Specifically, firstly the standard deviation of the liquid column velocity $\sigma_{\dot{Y}}$ is evaluated by fixing an arbitrary value of ζ_l, as

$$\sigma_{\dot{Y}}^2=\int_0^\infty\omega^2|H_Y(\omega)|^2G_0\,\mathrm{d}\omega,\tag{9}$$

in which $H_Y(\omega)$ is the liquid column displacement transfer function of the equivalent linear system (7) (see Appendix A for further details) and G_0 is the one-sided power spectral density (PSD) of the white noise ground excitation. Further, substituting $\sigma_{\dot{Y}}$ evaluated by Eq. (9) into Eq. (8) yields a new value of ζ_l. This procedure is repeated iteratively until no significant differences on ζ_l emerge in two consecutive iterations.

Clearly, once convergence is reached, the complete statistics of the response processes can be computed. In particular, defining $H_b(\omega)$ as the base-isolation subsystem displacement transfer function and $H_{X_1}(\omega)$ the main structure nodal deformation transfer function of the equivalent linear system (7) (see Appendix A for details), response variances are obtained as

$$\sigma_{X_b}^2=\int_0^\infty|H_b(\omega)|^2G_0\,\mathrm{d}\omega,\quad\sigma_{X_1}^2=\int_0^\infty\left|H_{X_1}(\omega)\right|^2G_0\,\mathrm{d}\omega,\quad\sigma_Y^2=\int_0^\infty|H_Y(\omega)|^2G_0\,\mathrm{d}\omega.\tag{10}$$

It should be noted that closed-form expression for these transfer functions can be easily computed, as reported in Appendix A. In this manner, all the response statistics can be immediately determined numerically solving Eq. (10).

In order to demonstrate the accuracy of the above-described iterative SLT, Fig. 2 shows the response steady-state variances of the original nonlinear equations of motion, Eq. (6), additionally to variances computed via Eq. (10) through the iterative procedure, for different values of the input PSD G_0. Note that statistics of the original nonlinear system (6) have been evaluated through a Monte Carlo simulation (MCS) procedure, using for each analysis 2000 samples of ground accelerations and directly integrating the equations of motion. In this respect, parameters similar to those used in [31] have been here adopted for the numerical simulations. Specifically: $\omega_b=\pi/2$, $\zeta_b=0.05$, $\mu_1=0.95$, $\omega_1=4\omega_b$, $\zeta_1=0.02$, $\mu_l=0.05$, $\alpha=0.6$, $\omega_l=0.98\omega_b$ and $\xi=10$. As it can be observed in this figure, base-isolation subsystem displacement variance $\sigma_{X_b}^2$ (Fig. 2a) and main structure displacement variance $\sigma_{X_1}^2$ (Fig. 2b), predicted with the iterative SLT, are in very good

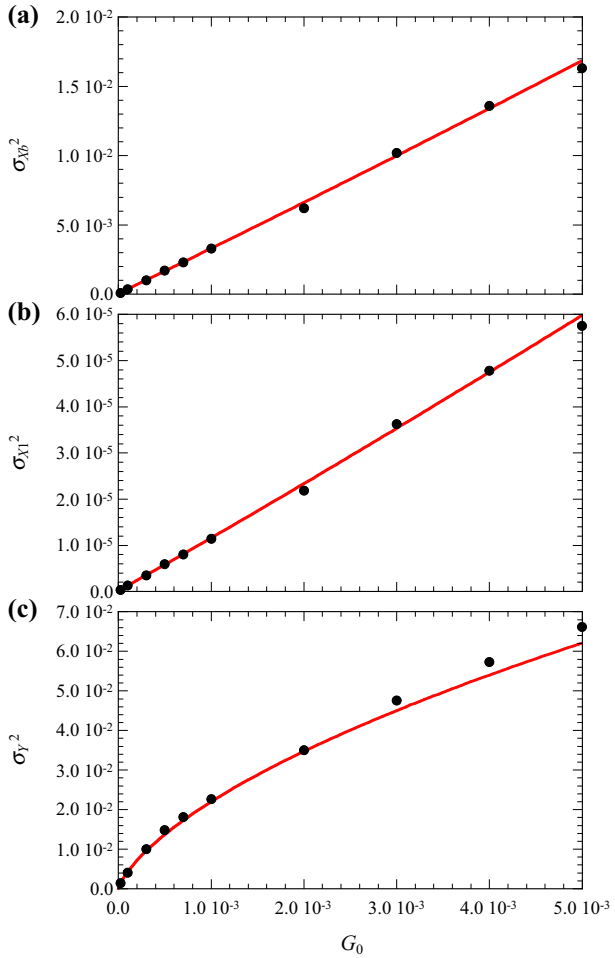

Fig. 2 Steady-state response variances versus input PSD: black circles—Monte Carlo simulation, red line—iterative standard linearization technique; **a** variance of the base-isolation subsystem displacements; **b** variance of the main structure displacements; **c** variance of the fluid displacements (color figure online)

agreement with those obtained by MCS on the nonlinear system (6), for a wide range of input PSD G_0, thus proving the reliability of the method. On the other hand, as depicted in Fig. 2c, since the nonlinear term in Eq. (6) involves the fluid velocity, less accurate agreement is reached for the fluid displacement variances σ_Y^2, at increasing values of the input PSD.

It is worth underscoring that, although the iterative procedure above described is well established in the literature [3,26,30] and leads to very accurate results in terms of statistics, the equivalent linear system must be found through several numerical evaluations. Hence, this procedure may not be suitable if one is interested in the assessment of the optimal design parameters of the TLCD, which are necessary to gather the highest control performances. Therefore, a direct procedure for the evaluation of the equivalent linear damping ratio ζ_l of the TLCD device should be sought. In this respect, in order to find a simplified straight relationship between the input PSD G_0 and the estimated value for ζ_l, a closed-form solution in terms of steady-state response statistic σ_Y^2 is proposed, as detailed in the following. This proposed procedure is based on the approach reported in [4,7], for TLCD-controlled systems, and here applied to deal with base-isolated TLCD hybrid-controlled SDOF structures, as those shown in Fig. 1c.

3 Direct evaluation of the equivalent linear system

It is well known that in well-designed base-isolated building the majority of the displacements occur within the base-isolation subsystem, while the main structure behaves virtually like a rigid body, with displacements

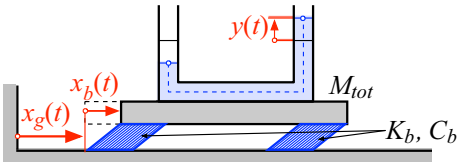

Fig. 3 Base-isolated rigid structure equipped with TLCD

orders of magnitude lower than those of the base-isolation subsystem itself [20,31]. It is therefore reasonable to further reduce the system, assuming that the entire base-isolated structure can be modeled as a SDOF linear system, as shown in Fig. 3. Thus, the original linear system (7) can be rewritten as

$$\begin{aligned}(1+\mu_l)\,\ddot{X}_b(t)+\alpha\mu_l\ddot{Y}+2\zeta_b\omega_b\dot{X}_b(t)+\omega_b^2X_b(t)&=-(1+\mu_l)\,\ddot{X}_g(t),\\ \alpha\ddot{X}_b(t)+\ddot{Y}(t)+2\zeta_l\omega_l\dot{Y}(t)+\omega_l^2Y(t)&=-\alpha\ddot{X}_g(t),\end{aligned}\tag{11}$$

which is now simply a set of two linear differential equations. In this way, the approach described in [7] can now be easily applied.

Specifically, expressing Eq. (11) in compact matrix form yields

$$\tilde{\mathbf{M}}\ddot{\mathbf{Z}}+\tilde{\mathbf{C}}\dot{\mathbf{Z}}+\tilde{\mathbf{K}}\mathbf{Z}=-\tilde{\mathbf{M}}\tilde{\mathbf{r}}\ddot{x}_g,\tag{12}$$

where $\mathbf{Z}=\left[\,X_b(t)\;Y(t)\,\right]^{\mathrm{T}}$, $\tilde{\mathbf{r}}=\left[\,1\;0\,\right]^{\mathrm{T}}$ and

$$\tilde{\mathbf{M}}=\begin{bmatrix}1+\mu_l & \alpha\mu_l\\ \alpha & 1\end{bmatrix},\quad \tilde{\mathbf{C}}=\begin{bmatrix}2\zeta_b\omega_b & 0\\ 0 & 2\zeta_l\omega_l\end{bmatrix},\quad \tilde{\mathbf{K}}=\begin{bmatrix}\omega_b^2 & 0\\ 0 & \omega_l^2\end{bmatrix}.\tag{13}$$

Since the input is modeled as a zero-mean stationary Gaussian white noise process, the corresponding Lyapunov equation of the evolution of the covariance matrix [4] can be written as

$$\dot{\Sigma}_{\mathbf{Q}}(t)=\mathbf{D_S}\Sigma_{\mathbf{Q}}(t)+\Sigma_{\mathbf{Q}}(t)\,\mathbf{D_s^T}+\mathbf{G_S}\mathbf{G_S^T}\pi G_0,\tag{14}$$

where $\mathbf{Q}=\left[\,\mathbf{Z}\;\dot{\mathbf{Z}}\,\right]^{\mathrm{T}}$ is the vector of the state variables, $\Sigma_{\mathbf{Q}}(t)$ represents the covariance matrix given as

$$\Sigma_{\mathbf{Q}}=\begin{bmatrix}\sigma_{X_b}^2 & \sigma_{X_bY}^2 & \sigma_{X_b\dot{X}_b}^2 & \sigma_{X_b\dot{Y}}^2\\ & \sigma_Y^2 & \sigma_{Y\dot{X}_b}^2 & \sigma_{Y\dot{Y}}^2\\ sym & & \sigma_{\dot{X}_b^2}^2 & \sigma_{\dot{X}_b\dot{Y}}^2\\ & & & \sigma_{\dot{Y}}^2\end{bmatrix},\tag{15}$$

while $\mathbf{D_S}$ and $\mathbf{G_S}$ are given as

$$\mathbf{D_S}=\begin{bmatrix}\mathbf{0} & \mathbf{I_2}\\ -\tilde{\mathbf{M}}^{-1}\tilde{\mathbf{K}} & -\tilde{\mathbf{M}}^{-1}\tilde{\mathbf{C}}\end{bmatrix},\quad \mathbf{G_S}=\begin{bmatrix}\mathbf{0}\\ \tilde{\mathbf{r}}\end{bmatrix}\tag{16}$$

with $\mathbf{I_2}$ a 2×2 identity matrix.

Solution of Eq. (14) yields the evolution of all the response statistics of the system described by Eq. (11). However, since only the steady-state variance must be computed, $\dot{\Sigma}_{\mathbf{Q}}$ can be equated to zero. In this way, after some algebra, the base-isolation subsystem displacement and the fluid column velocity variances can be expressed as

$$\sigma_{X_b}^2=\frac{\pi G_0}{4z_{X_b}\omega_b^3},\quad \sigma_{\dot{Y}}^2=\frac{\pi G_0}{4z_Y\omega_l},\tag{17}$$

in which z_{X_b} and z_Y have the following expression

$$z_{X_b}=\frac{N_Z}{D_{ZX_b}},\quad z_Y=\frac{N_Z}{D_{ZY}},\tag{18}$$

where

$$\begin{aligned} N_Z &= \zeta_b\zeta_l + \zeta_2^2\left(4\zeta_b^2 + \alpha^2\mu_l\right)\nu + 2\zeta_b\zeta_l\left[2\zeta_b^2 + \alpha^2\mu_l + \left(2\zeta_l^2 - 1\right)(1+\mu_l)\right]\nu^2 \\ &\quad + \zeta_b^2\left[\alpha^2\mu_l + 4\zeta_l^2(1+\mu_l)\right]\nu^3 + \zeta_b\zeta_l(1+\mu_l)^2\nu^4, \\ D_{ZX_b} &= \zeta_l\left(1+\mu_l-\alpha^2\mu_l\right)^2 \\ &\quad + \zeta_b\left[\alpha^4\mu_l^2 + 4\zeta_l^2(1+\mu_l)^2\right]\nu + \zeta_l(1+\mu_l)^2\left[4\zeta_b^2 + 3\alpha^2\mu_l + \left(4\zeta_l^2 - 2\right)(1+\mu_l)\right]\nu^2 \\ &\quad + \zeta_b(1+\mu_l)^2\left[\alpha^2\mu_l + 4\zeta_l^2(1+\mu_l)\right]\nu^3 + \zeta_l(1+\mu_l)^4\nu^4, \\ D_{ZY} &= \alpha^2\left[\zeta_b + \zeta_l\left(1+\mu_l+4\zeta_b^2\right)\nu + 4\zeta_b^3\nu^2\right], \end{aligned} \tag{19}$$

and the so-called frequency tuning ratio $\nu = \omega_l/\omega_b$ has been introduced.

By application of the procedure described in [4,7], in order to obtain a less cumbersome expression for the fluid velocity variance, Eq. (19b) can be expanded in Taylor's series with respect to ζ_l, retaining only the first two terms of the expansion. Further, assuming that higher powers of ζ_b can be neglected $\left(\zeta_b^2 = \zeta_b^3 \approx 0\right)$, and considering that generally $\nu \approx 1$, yields

$$z_Y \approx (\zeta_b + \gamma\zeta_l)\,\mu_l, \tag{20}$$

where $\gamma = 1 - \mu_l + \mu_l/\alpha^2$. Substitution of Eq. (20) into Eq. (17b) leads to an approximate expression for the fluid velocity variance,

$$\sigma_{\dot{Y}}^2 = \frac{\pi G_0}{4\,(\zeta_b + \gamma\zeta_l)\,\mu_l\omega_l}. \tag{21}$$

Finally, recalling Eq. (8), a direct relationship that provides the equivalent damping ratio ζ_l as a function of the input PSD G_0 can be obtained as

$$\zeta_l^2\,(\zeta_b + \gamma\zeta_l) = \frac{\xi^2 G_0}{8L^2\,\mu_l\,\nu\omega_b^3}, \tag{22}$$

in which ω_l has been replaced by the term $\nu\omega_b$. This third order algebraic equation, which can be solved either numerically or in closed form, admits only one real solution in the parameters range of practical applications [4]. Therefore, if the base-isolation subsystem and TLCD parameters are known, Eq. (22) can be directly used to evaluate ζ_l instead of applying the computationally more expensive iterative SLT procedure previously described.

On the other hand, recalling that $\omega_l^2 = 2g/L$ [34], an expression relating the head loss coefficient ξ to the equivalent damping ratio ζ_l can be obtained recasting Eq. (22) as

$$\xi = \frac{\xi_0\,(\nu, \zeta_l)}{\sqrt{G_0\omega_b}}, \tag{23}$$

where

$$\xi_0\,(\nu, \zeta_l) = 4g\zeta_l\sqrt{\frac{2\mu_l\,(\zeta_b + \gamma\zeta_l)}{\nu}}. \tag{24}$$

Note that Eqs. (23) and (24) are rather useful for a straightforward evaluation of the optimal TLCD design parameters, as it will be shown in the following.

3.1 Investigation on parameter sensitivity

In order to prove the reliability of the proposed direct approach for the evaluation of equivalent TLCD damping parameter ζ_l, it will be shown how the variation of the involved parameters affects the proposed formulation. To aim at this objective, a reference set of parameters, used also in [31], has been selected, and in turn one of them has been varied in a wide range of values. Specifically, the following reference set of parameters is used: $\omega_b = \pi/2$, $\zeta_b = 0.05$, $\mu_1 = 0.95$, $\omega_1 = 4\omega_b$, $\zeta_1 = 0.02$, $\mu_l = 0.05$, $\alpha = 0.6$, $\xi = 10$, and $G_0 = 5 \times 10^{-4}$.

In the following figures, results in terms of normalized base-isolation displacement variance $\varepsilon_{X_b} = \sigma_{X_b}^2/\sigma_{X_0}^2$ are displayed, being $\sigma_{X_0}^2$ the base-isolation displacement variance of the system without TLCD (see Eq. (4)). In particular, results obtained by the iterative SLT previously described (symbols) are compared with those obtained by the proposed direct approach (solid lines), for tuning ratio $\nu = \omega_l/\omega_b$ ranging from 0.8 to 1.2.

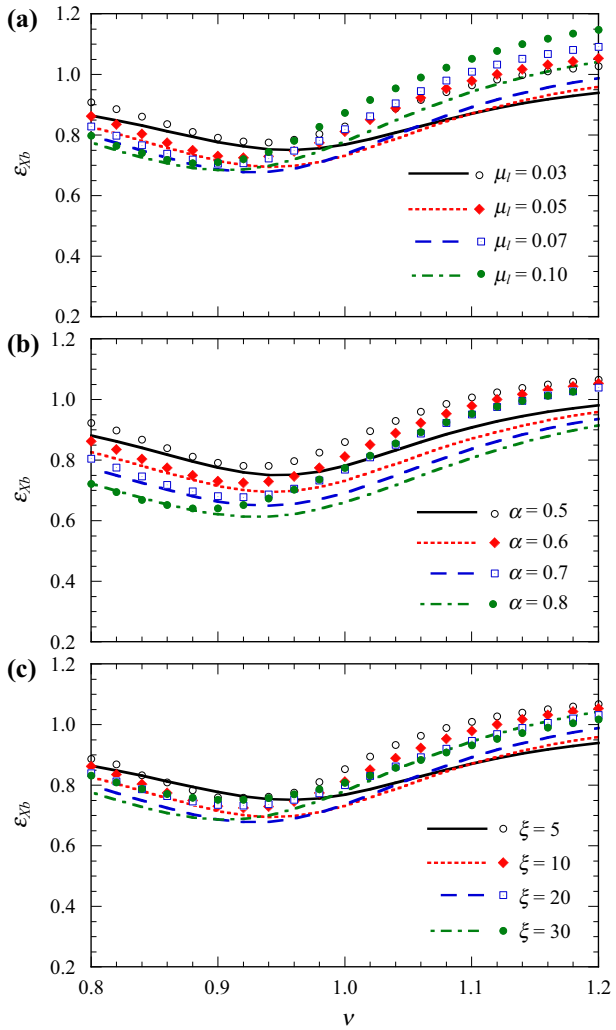

Fig. 4 Normalized base-isolation subsystem displacement variance ε_{X_b} as a function of frequency tuning ratio ν: markers—iterative standard linearization technique; lines—proposed direct approach; **a** variation of the mass ratio μ_l; **b** variation of the length ratio α; **c** variation of the head loss coefficient ξ

In Fig. 4, the effects of the variation of mass ratio μ_l, length ratio α and the head loss coefficient ξ on the proposed formulation are shown. As it can be observed, better agreement between iterative SLT and proposed approach is attained for values of the tuning ratio ν lower than one, otherwise higher deviations can be detected. Further, as shown in Figs. 4a, b, the proposed procedure is slightly influenced by the variation of μ_l and α, while the accuracy of the results significantly decreases for higher values of ξ (see Fig. 4c).

In Fig. 5, similar results are reported for the variation of the base-isolation subsystem damping ratio ζ_b, the main structure damping ratio ζ_1 and the input PSD G_0. As for the previous cases, better agreement is obtained for values of the tuning ratio ν lower than one. In this case, however, the accuracy of the results decreases for higher values of ζ_b (see Fig. 5a) and G_0 (see Fig. 5c). On the other hand, as shown in Fig. 5b, no significant influence of the main structure damping ratio ζ_1 on ϵ_{X_b} can be observed.

Moreover, as shown in Fig. 5a, the normalized base-isolation displacement variance ϵ_{X_b} is greatly influenced by parameter ζ_b, meaning that highest control performance can be reached for low-damped base-isolation subsystems, as expected.

It should be emphasized that, while the iterative SLT procedure takes into account the main structure damping ratio ζ_1, being developed on the complete equivalent linear system described by Eq. (7), the proposed direct approach is developed on the reduced system in Eq. (11), which is therefore independent of ζ_1. The latter is a remarkable result that makes the proposed procedure valid for hybrid-controlled MDOF structures as well.

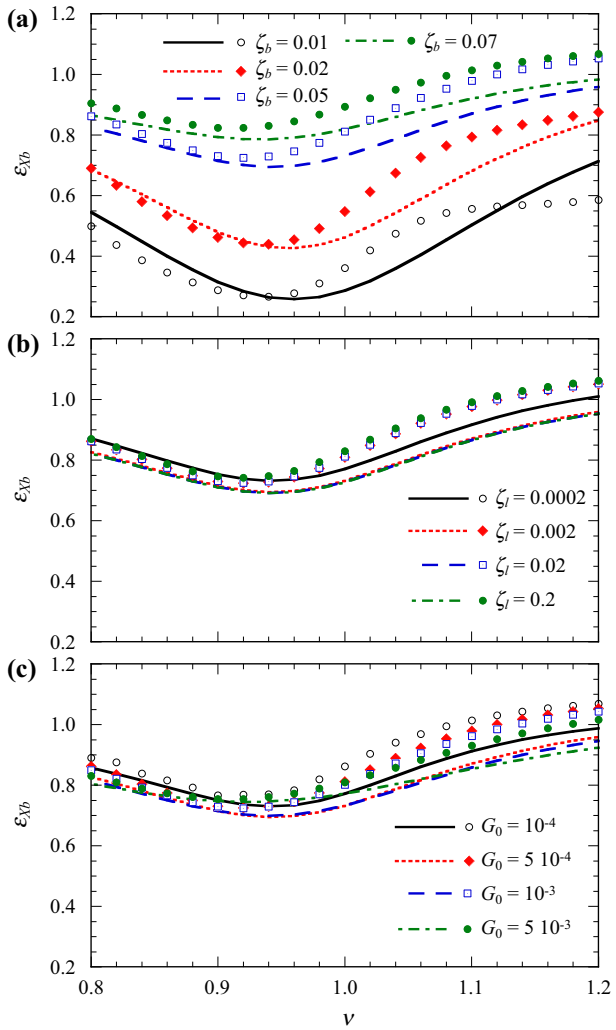

Fig. 5 Normalized base-isolation displacement variance ε_{X_b} as a function of frequency tuning ratio ν: Markers—iterative standard linearization technique; Lines—proposed direct approach; **a** variation of the base-isolation damping ratio ζ_b; **b** variation of the main structure damping ratio ζ_1; **c** variation of the input PSD G_0

Finally, it should be underscored that, although some discrepancies between the iterative SLT and the proposed direct approach have been evidenced from the above analyses, the main purpose of the proposed procedure is to quickly derive the optimal design parameters of the TLCD device, as it will be shown in the following.

4 Optimal design parameters of TLCD systems

Once the expression directly linking ζ_l to the excitation PSD G_0 has been introduced, the optimal design of TLCD devices for base-isolated structures can be effectively performed using the proposed approximate formulation. As customary, there is no need for an optimization procedure that includes all the TLCD involved parameters, since μ_l and α are generally given by structural constraints. Therefore, the only parameters requested are the frequency tuning ratio ν and the head loss coefficient ξ, or similarly the equivalent damping ratio ζ_l. Clearly, the real optimal parameters should be evaluated on the original nonlinear system (6), or more easily on the equivalent linear equation (7), with ζ_l estimated through the iterative procedure previously described. It is worth noting that both these approaches are rather laborious and cannot be pursued in practical application. In fact, the evaluation of the optimal parameters on the original nonlinear system (6) requires a computationally demanding MCS, necessary to compute the statistics of the system for different values of

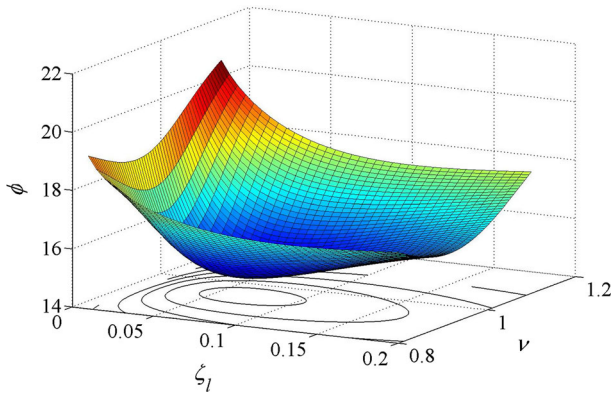

Fig. 6 Sample of the smooth function $\phi\,(\nu, \zeta_l)$

the design parameters, until a minimum of $\sigma^2_{X_b}$ is reached for a certain set of values of (ν, ξ). Further, the evaluation of the optimal parameters on the equivalent linear system (7) requires a rather cumbersome numerical optimization, which must take into account the iterative procedure necessary to estimate the equivalent damping ratio ζ_l. On the other hand, Eq. (17a) directly expresses the base-isolation subsystem displacement variance $\sigma^2_{X_b}$ of the reduced equivalent linear system in Eq. (11), as function of the input PSD G_0 and the system parameters. Therefore, a more practical and straightforward approach is to look for the minimum of the smooth function

$$\phi\,(\nu, \zeta_l) = \frac{1}{z_{X_b}}, \tag{25}$$

which is independent of G_0 and the natural base-isolation system frequency ω_b. In Fig. 6, a sample of the function $\phi\,(\nu, \zeta_l)$ is shown.

Note that an analytical expression for the minimum of $\phi\,(\nu, \zeta_l)$ could be obtained, considering the nonlinear system of algebraic equations

$$\frac{\partial \phi\,(\nu, \zeta_l)}{\partial \nu} = 0\ , \quad \frac{\partial \phi\,(\nu, \zeta_l)}{\partial \zeta_l} = 0 \tag{26}$$

However, this approach would lead to a rather complex expression, and thus, it is here omitted.

A more simple procedure is to directly find numerically the minimum of $\phi\,(\nu, \zeta_l)$ in Eq. (25), through numerical minimization procedure, such as those already implemented in many software packages (see, for instance, *FindMinimum* in Mathematica or *fminsearch* in MATLAB environment). In this way, Eq. (25) provides the optimal design parameter values ν_{opt} and $\zeta_{l,\text{opt}}$, which can be then used to compute the optimal head loss coefficient ξ_{opt} through Eq. (23) with $\xi_0\left(\nu_{\text{opt}}, \zeta_{l,\text{opt}}\right)$ given by Eq. (24).

As it will be shown in the following, application of the above- described procedure results in a significant reduction in computational effort, leading to optimized values that have almost the same performances as those obtained through the computationally demanding iterative procedure.

4.1 Investigation on the optimal design parameters

The main advantage of the proposed approach lies in the straightforward evaluation of the optimal values ν_{opt} and $\zeta_{l,\text{opt}}$, which are independent of input PSD G_0 and natural base-isolation frequency ω_b. Therefore, this procedure can be used to create immediately useful design charts, in which optimal parameters can be directly determined. Specifically, the charts depicted in Fig. 7 show optimal values in terms of $\xi_0\left(\nu_{\text{opt}}, \zeta_{l,\text{opt}}\right)$ and ν_{opt}, for different values of α. Further, several values of the base-isolation damping ratio ζ_b (black lines) and mass ratio μ_l (red lines) are depicted. The here proposed charts render the optimization procedure particularly easy. For instance, suppose that a length ratio $\alpha = 0.6$ is taken into account, the damping ratio of the base-isolated system is $\zeta_b = 0.02$ and the mass ratio, given by structural constraints, is $\mu_l = 4\%$, thus identifying the point **A** in Fig. 7b. This design chart directly provides the optimal parameters $\nu_{\text{opt}} = 0.964$ and $\xi_0\left(\nu_{\text{opt}}, \zeta_{l,\text{opt}}\right) = 0.192$, which can then be substituted into Eq. (23) to find the optimal head loss coefficient ξ_{opt}, once the input PSD G_0 is known.

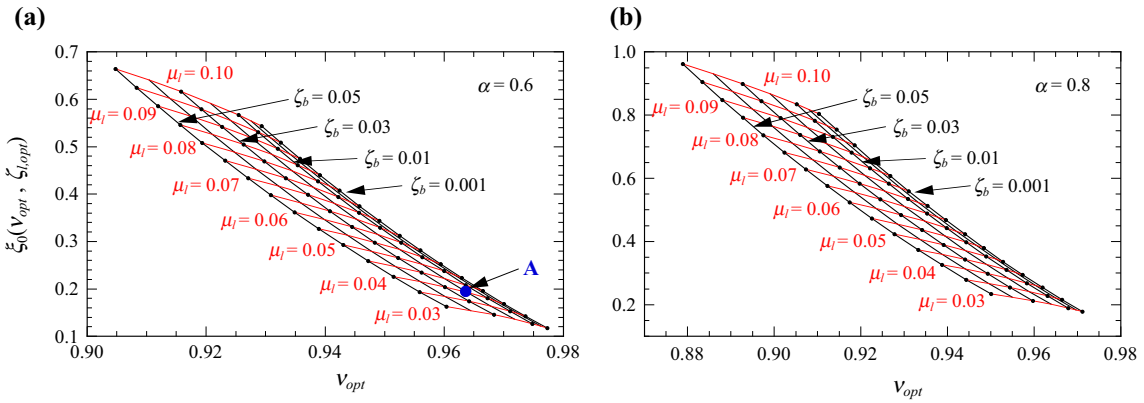

Fig. 7 Optimal design charts in terms of $\xi_0\left(\nu_{\text{opt}}, \zeta_{l,\text{opt}}\right)$ and ν_{opt}; **a** $\alpha = 0.6$; **b** $\alpha = 0.8$

At this stage, it is worth noting that the above-described procedure can be still applied even for generic earthquake excitation, defined in the specific seismic code in terms of spectral acceleration response spectrum, as it will be shown in the following and further detailed in [7].

Finally, in order to show the accuracy of this proposed simplified approach, a comparison with the optimal values obtained through the iterative SLT has also been performed. In this respect, considering the previously introduced reference set of parameters (see Sects. 3.1), which in turn have been varied in a wide range of values, the particle-swarm optimization (PSO) method [23] has been used to find those values of (ν, ξ) that minimize the base-isolation displacement variance $\sigma^2_{X_b}$ of the complete linear equations of motion (7). Note that, in this way, for each iteration of the PSO optimization algorithm the iterative SLT must be applied to evaluate the equivalent linear damping ratio ζ_l, as previously discussed. Therefore, in this case, a rather elaborate numerical procedure must be implemented.

In Table 1, the comparison among the optimal design parameters ν_{opt} and ζ_{opt}, obtained by the proposed simplified approach, and those determined through the aforementioned iterative solution, is listed for various values of the system parameters, together with the corresponding percentage differences. For the results of this table, the following reference set of values has been used: $\alpha = 0.06$, $\mu_l = 0.05$, $\zeta_b = 0.05$, $\zeta_1 = 0.01$, $G_0 = 5 \times 10^{-4}$.

Furthermore, Table 1 also provides the previously defined normalized base-isolation subsystem displacement variance $\varepsilon_{X_b} = \sigma^2_{X_0}/\sigma^2_{X_0}$, where $\sigma^2_{X_0}$ is the base-isolation subsystem displacement variance of the system without TLCD (see Eq. 4). Note that this parameter may also serve as a performance control index for the base-isolated TLCD-controlled structure, since the lower ε_{X_b} is, the more effective the TLCD has been. As shown in Table 1, very small differences between the two approaches are obtained in terms of optimal tuning ratio ν_{opt}. On the other hand, higher discrepancies are achieved in terms of the optimal head loss coefficient ξ_{opt}, especially for greater values of ζ_b. However, as highlighted in the last columns of Table 1, very small differences between the two procedures exist in terms of the parameter ε_{X_b}, with the largest error being less than 5%. Clearly, as expected, the fact that these errors are always negative means that higher control is reached with optimal parameters evaluated through the iterative procedure.

Nevertheless, since very small discrepancies are obtained in terms of ε_{X_b}, and considering the significant reduction in computational effort achieved with the proposed straightforward procedure, the aforementioned approach can effectively be regarded as a powerful and reliable tool to be employed for the evaluation of the optimal design parameters.

5 Analysis of control performance

In the previous analysis, a stationary white noise process has been considered as a model for the base acceleration, with the aim of deriving the optimal design parameters minimizing the computational cost. Clearly, real earthquake ground motions are neither stationary nor have a constant PSD as in the case of the white noise. Therefore, to show the influence of the non-stationary nature of real ground motions, in this section the control performances of the base-isolated structure with attached TLCD device are examined by using time-history analyses with selected recorded accelerograms.

Table 1 Comparison of optimal TLCD design parameters ν_{opt} and ξ_{opt} Reference set of values: $\alpha = 0.06$, $\mu_l = 0.05$, $\zeta_b = 0.05$, $\zeta_1 = 0.01$, $G_0 = 5 \times 10^{-4}$

		ν_{opt} Proposed approach	ν_{opt} Iterative solution	Err. (%)	ξ_{opt} Proposed approach	ξ_{opt} Iterative solution	Err. (%)	ε_{X_b} Proposed approach	ε_{X_b} Iterative solution	Err. (%)
α	0.5	0.949	0.928	− 2.35	8.34	10.01	16.7	0.79	0.78	− 1.03
	0.6	0.943	0.919	− 2.51	10.4	12.07	13.7	0.73	0.72	− 1.02
	0.7	0.936	0.914	− 2.40	12.7	14.05	9.86	0.68	0.67	− 0.99
	0.8	0.928	0.908	− 2.17	15.1	16.58	9.10	0.63	0.62	− 0.77
μ_l	0.03	0.960	0.937	− 2.43	5.79	6.83	15.2	0.78	0.77	− 1.66
	0.05	0.943	0.920	− 2.47	10.4	12.3	15.2	0.73	0.72	− 1.02
	0.07	0.927	0.907	− 2.17	15.5	16.9	8.51	0.69	0.69	− 0.86
	0.10	0.905	0.887	− 1.98	23.7	24.7	4.06	0.67	0.66	− 0.58
ζ_b	0.01	0.959	0.941	− 1.98	8.46	7.81	−8.38	0.33	0.32	− 4.13
	0.02	0.956	0.939	− 1.85	8.97	9.18	2.25	0.46	0.45	− 2.27
	0.05	0.943	0.920	− 2.47	10.4	12.5	16.8	0.73	0.72	− 1.02
	0.07	0.932	0.911	− 2.35	11.3	14.1	19.9	0.82	0.82	− 0.69
ζ_1	0.0002	0.943	0.921	− 2.39	10.4	12.4	15.6	0.73	0.72	− 0.99
	0.002	0.943	0.921	− 2.34	10.4	12.3	15.0	0.73	0.72	− 1.00
	0.02	0.943	0.921	− 2.42	10.4	12.3	15.2	0.73	0.72	− 1.02
	0.2	0.943	0.918	− 2.69	10.4	12.5	16.7	0.75	0.74	− 1.20
G_0	1×10^{-4}	0.943	0.943	− 2.40	23.3	27.1	14.0	0.73	0.72	− 1.02
	5×10^{-4}	0.943	0.920	− 2.44	10.4	12.2	14.8	0.73	0.72	− 1.02
	1×10^{-3}	0.943	0.919	− 2.52	7.37	8.83	16.6	0.73	0.72	− 1.02
	5×10^{-3}	0.943	0.920	− 2.47	3.29	3.84	14.2	0.73	0.72	− 1.02

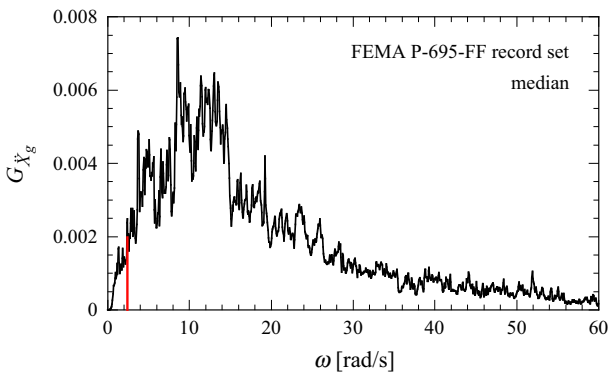

Fig. 8 Median of the PSDs of the 44 records of the FEMA P-695-FF set

Specifically, results are based on the 44 recorded far-field ground motions of the FEMA P-695-FF set described in [10], which originate from severe seismic events of moment magnitude between 6.5 and 7.6 recorded on NEHRP site classes C (soft rock) and D (stiff soil). The structural properties of each story unit are as follows: story mass $M_i = 300 \times 10^3$ kg, elastic story stiffness $K_i = 10^6$ kN/m, damping coefficient $C_i = 2261$ kN s/m (corresponding to a damping ratio of the first mode $\zeta_1 = 0.005$), and height of each story $h_i = 3.0$ m. As far as the base-isolation system is concerned, its mass is $M_b = 400 \times 10^3$ kg, while stiffness and damping coefficient are assumed to be, respectively, $K_b = 40 \times 10^3$ kN/m (corresponding to a natural frequency $\omega_b = 2.5$ rad/s) and $C_b = 90.44$ kN s/m (corresponding to a damping ratio $\zeta_b = 0.0028$). Further, in order to properly design the TLCD device to be connected to the base-isolated structure, the one-sided PSD $G_{\ddot{X}_g}(\omega)$ of the FEMA P-695-FF record set has been computed, thus determining the corresponding value of the input PSD $G_0 = G_{\ddot{X}_g}(\omega_b)$. The median of the PSDs of these records is shown in Fig. 8. For the analysis, the PSD at ω_b is taken, i.e., $G_0 = 0.002$, see Fig. 8. The benchmark structure considered for the numerical analysis is a base-isolated 20-story shear-type planar frame ($n = 20$), used in [33]. Therefore, considering a TLCD with mass ratio $\mu_l = 5\%$ and length ratio $\alpha = 0.8$, the optimal design parameters obtained by proposed simplified approach are $\nu_{\text{opt}} = 0.952$ and $\xi_{\text{opt}} = 4.71$.

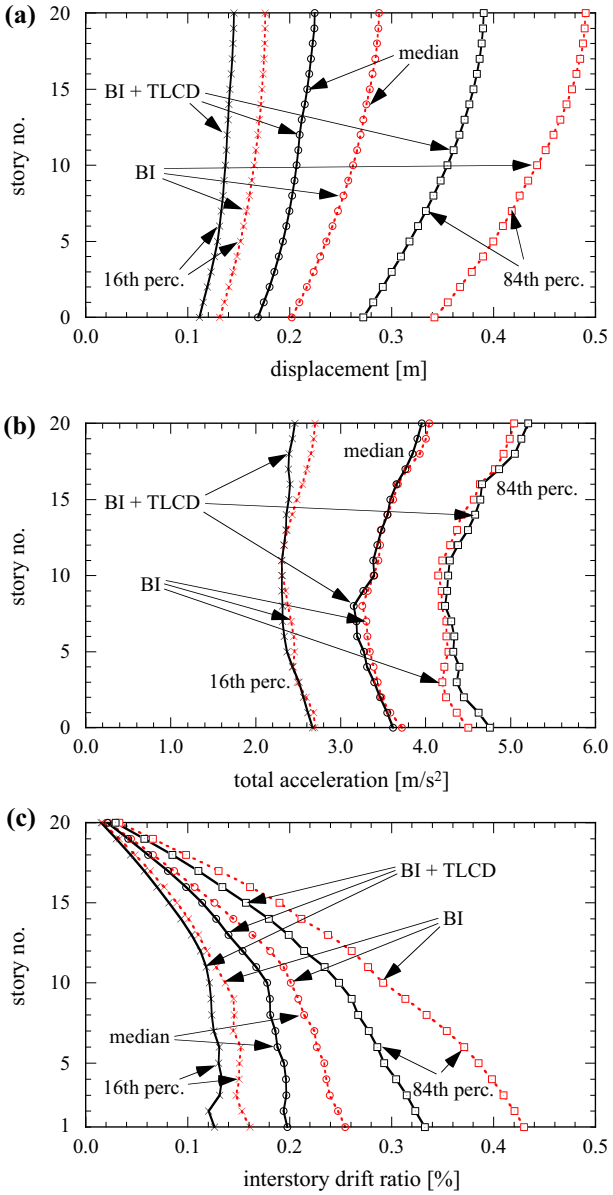

Fig. 9 Response profiles for hybrid-controlled structure (BI + TLCD—black solid line) and base-isolated structure (BI—red dashed line) subjected to the 44 FEMA P-695-FF records: circles—median; crosses—16th percentile; squares—84th percentiles; **a** peak floor displacement relative to the ground; **b** peak floor total acceleration; **c** peak floor interstory drift ratio (color figure online)

To properly account for the non-classical damping nature of the base-isolated structure and the nonlinear features of the TLCD device, direct numerical solution of the pertinent equations of motion of the complete systems (Eqs. (3) and (5)) has been performed using a forth order Runge–Kutta algorithm, using as base accelerations the FEMA P-695-FF records. In this manner, for each of the FEMA P-695-FF 44 records, the displacement relative to the ground, total acceleration and interstory drift ratio of the base-isolation subsystem and story beams have been determined for both the base-isolated structure and the base-isolated structure controlled by TLCD device.

In this regard, Fig. 9 shows comparison of the profile of the median of the peak response quantities of the base-isolated structure with (black solid line) and without (red dashed line) TLCD. Further, for the sake of completeness, the corresponding 16th and 84th percentiles are also depicted. As apparent in these figures, the optimized TLCD device directly connected to the base-isolation subsystem is able to effectively reduce

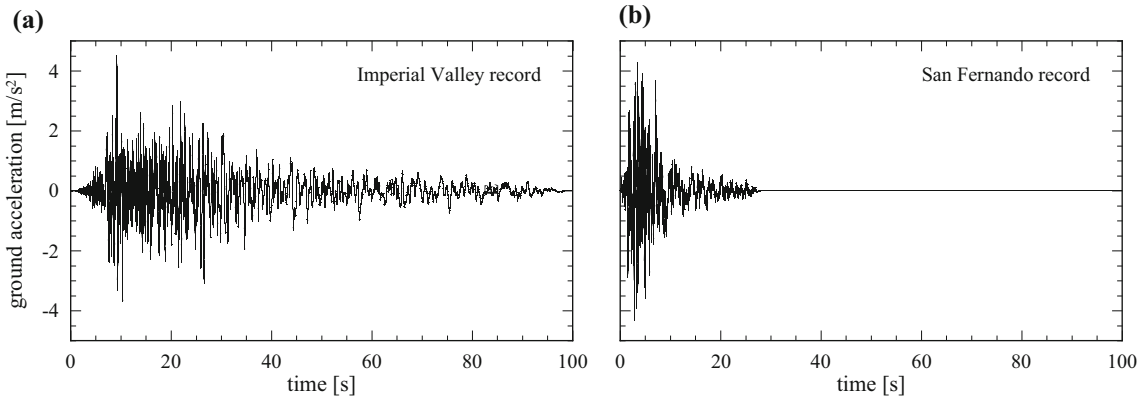

Fig. 10 Two accelerograms of the FEMA P-695-FF record set: **a** Imperial Valley record; **b** San Fernando record

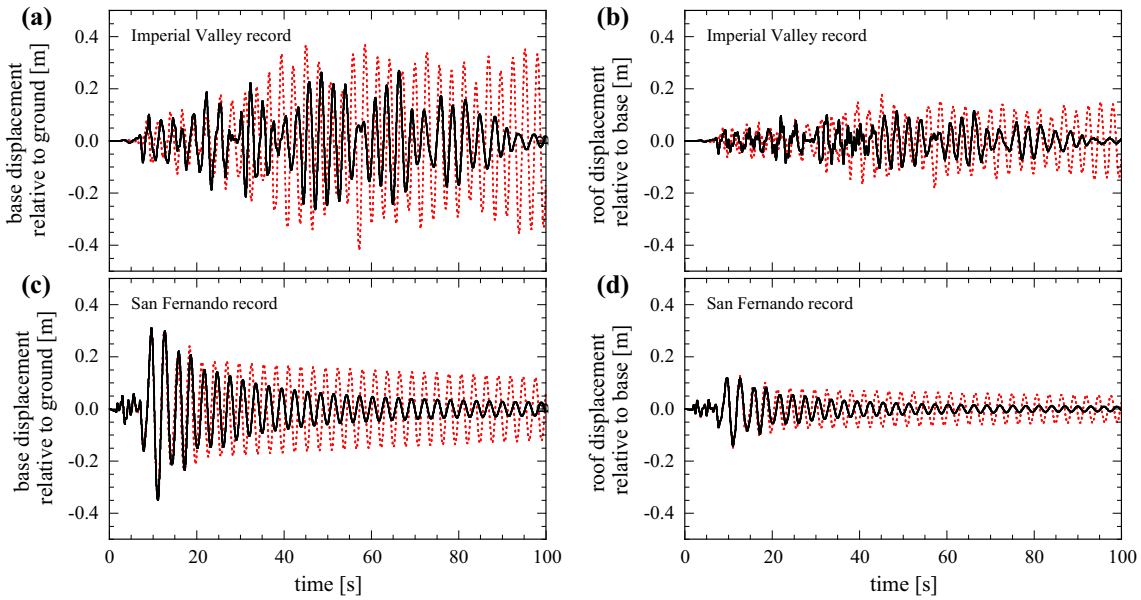

Fig. 11 Response time histories of hybrid-controlled structure (black solid line) and base-isolated structure (red dashed line) subjected to the **a**, **b** Imperial Valley and **c**, **d** San Fernando earthquake records; **a**, **c** base-isolation displacement relative to ground; **b**, **d** roof displacement relative to base-isolation (color figure online)

the relative displacement demand (Fig. 9a), with a reduction in the median of 16% at the base plate and 22% at the roof. The total peak accelerations remain almost unaffected by the TLCD, as shown in Fig. 9b. It is also worth stressing that, since the interstory drift ratios decrease when a TLCD device is connected to the base-isolation subsystem (see Fig. 9c), this reduction is not achieved at their expense, as may happen when generally providing supplemental damping to the base-isolation subsystem [17,27].

Analogous results may also be seen from the time histories of all the response quantities. However, from a thorough analysis of the responses to each of the 44 records, it can be evidenced that there may be cases in which the TLCD has little effect in reducing the displacement demand of the base-isolation system. In this respect, two records of the considered FEMA P-695-FF record set, specifically the Imperial Valley and the San Fernando earthquakes, are depicted in Fig. 10, while comparison among the corresponding response time histories of the base-isolated benchmark structure with and without TLCD are shown in Fig. 11.

As evident from Fig. 11a, for the Imperial Valley earthquake record, the TLCD device yields a clear reduction in the peak base-isolation displacement (relative to the ground) of almost 35% . Further, similar features can be observed for the roof displacement (relative to the base-isolation) (Fig. 11b).

On the other hand, as shown in Figs. 11c, d, a different behavior is noticeable considering the San Fernando earthquake record. In this case, the TLCD device yields no reduction at all in terms of peak base-isolation

subsystem displacement, even though it clearly leads to a more rapid dissipation of the free vibration response (Fig. 11c). This phenomenon is rather common to other similar systems, such as TMD controlled structures [28] or TMD controlled base-isolated structures [27,29]. Specifically, this is due to the fact that passive control devices (as TLCDs and TMDs) have little effects on the structural responses in the first few seconds of the excitation. Therefore, TLCDs cannot appreciably reduce maximum base-isolation subsystem displacement if the maximum response occurs early in the earthquake record, as in the case of the San Fernando ground motion. For such excitation, the use of an active TLCD device would be recommended [14,19,32]. Nevertheless, since the overall effect of the TLCD on the base-isolation system, for the considered FEMA P-695-FF record set, is a clear reduction in all structural displacement and drift ratio demands, as already highlighted in Fig. 9, this passive control device appears to be rather effective in decreasing the displacement demand of the base-isolation subsystem. Moreover, taking into account the previously described TLCD-positive features (easy installation, low maintenance, mass of water utilizable for firefighting too), and considering that such a device would be positioned on the ground level, the proposed TLCD-controlled base-isolated structure is simple enough for practical implementation, when a reduction in the displacement demand of the base-isolation system is required.

6 Conclusions

In this paper, the effect of a tuned liquid column damper (TLCD) device on the seismic response of base-isolated structures has been investigated. The pertinent equations of motion of a multi-degree-of-freedom (MDOF) base-isolated structure, controlled at the base through a TLCD, have been introduced. Considering a Gaussian white noise model of the ground excitation, and under some assumptions regarding the base-isolation subsystem, a straightforward procedure for the optimal design of such a device has been proposed, aiming at maximally control the seismic response of the base-isolated structure. In order to prove the reliability of the proposed approach, comparison with the classical iterative statistical linearization technique (SLT) has been presented, showing a satisfactory agreement between the two approaches, even when the aforementioned assumptions are removed.

On this base, a direct optimization procedure of the TLCD design parameters has been performed, and optimal design charts have been introduced as a ready-to-use practical design tool. Comparison with the optimal parameters obtained by a rather elaborate numerical optimization procedure, based on the classical iterative SLT, has been carried out, leading to very small discrepancies especially in terms of control performances. Note, however, that a significant reduction in computational effort has been achieved with the proposed straightforward approach.

To show the influence of the non-stationary nature of real ground motions, the control performance of the TLCD device connected to the base-isolated structure has been examined, employing time-history analyses using the 44 recorded ground motions of the FEMA P-695 far-field set, and considering a 20-story benchmark base-isolated shear-type frame structure. It has been shown that the TLCD device can lead to a 16% reduction in the median of the peak base-isolation displacement, compared to the base-isolated structure without TLCD. It is also worth stressing that similar reduction has been reached for other response quantities, such as roof peak displacement and interstory drift ratio. However, the total acceleration demands remain almost unaffected by the TLCD. Further, from the time-history analyses it has been found that, although the TLCD has moderate effect on the peak response in case of earthquake records with early large pulse (as also happens with other passive control devices), it can add damping to the structure to reduce the subsequent free vibration response.

For sake of simplicity, the main structure and the base-isolation subsystem have been assumed to be linear elastic. Clearly, many real base-isolation systems may show characteristic nonlinear features. Nevertheless, the herein developed analysis would be equally applicable by utilizing, for instance, an equivalent linearization technique to partially take into account for the effect of the nonlinearity.

Finally, considering the advantageous characteristics of the TLCD devices and its overall beneficial effects in controlling the seismic response of base-isolated structures, TLCDs can be regarded as a practical and appealing means to reduce the displacement demands of the base-isolation subsystem. In any case, it is hoped that results presented in this paper provide valuable insights to researchers and engineers contemplating the use of TLCDs in base-isolated structures.

7 Appendix A

In this appendix, the displacement transfer functions of the equivalent linear equations of motion (7) are presented. In this respect, the Fourier transform of system (7) yields

$$
\begin{aligned}
&X_b(\omega)\left[-\omega^2(1+\mu_l)+2i\omega\zeta_b\omega_b+\omega_b^2\right]-\omega^2\alpha\mu_l Y(\omega)-\omega^2\mu_1 X_1(\omega)=-(1+\mu_l)\ddot{X}_g(\omega),\\
&-\omega^2\alpha X_b(\omega)+Y(\omega)\left[-\omega^2+2i\omega\zeta_l\omega_l+\omega_l^2\right]=-\alpha\ddot{X}_g(\omega),\\
&-\omega^2 X_b(\omega)+X_1(\omega)\left[-\omega^2+2i\omega\zeta_1\omega_1+\omega_1^2\right]=-\ddot{X}_g(\omega).
\end{aligned}
\tag{27}
$$

Therefore, the base-isolation displacement transfer function ($H_b(\omega)=X_b(\omega)/\ddot{X}_g(\omega)$) can be written as

$$
H_b(\omega)=\frac{(1+\mu_l)+\frac{\omega^2\alpha^2\mu_l}{c(\omega)}+\frac{\omega^2\mu_l}{a(\omega)}}{-b(\omega)+\frac{\omega^4\alpha^2\mu_l}{c(\omega)}+\frac{\omega^2\mu_l}{a(\omega)}},
\tag{28}
$$

while the main structure displacement transfer function ($H_{X_1}(\omega)=X_1(\omega)/\ddot{X}_g(\omega)$) and liquid column displacement transfer function, respectively, are

$$
H_{X_1}(\omega)=\frac{1}{a(\omega)}\left[-1+\omega^2 H_b(\omega)\right],\ H_Y(\omega)=\frac{\alpha}{c(\omega)}\left[-1+\omega^2 H_b(\omega)\right]
\tag{29}
$$

in which

$$
a(\omega)=-\omega^2+i\omega 2\zeta_1\omega_1+\omega_1^2,\ b(\omega)=-\omega^2(1+\mu_l)+i\omega 2\zeta_b\omega_b+\omega_b^2,\ c(\omega)=-\omega^2+i\omega 2\zeta_l\omega_l+\omega_l^2.
\tag{30}
$$

These parameters can be directly used to evaluate the statistics of the equivalent linear system in Eq. (7), necessary for the iterative SLT.

Acknowledgements Open access funding provided by University of Innsbruck and Medical University of Innsbruck.

References

1. Adam, C., Hruska, A., Kofler, A.: Elastic structures with tuned liquid column dampers. In: M. Durakbasa, A. Afjehi, P. Osanna (eds.) Proceedings of the of the XVI IMEKO (International Measurement Confederation) World Congress, vol. VII, pp. 351–356 (2000)
2. Arfiadi, Y., S, H.M.N.: Hybrid base isolation-passive mass damper systems. In: Computing in Civil and Building Engineering, pp. 279–286. Stanford, USA (2000)
3. Chang, C.: Mass dampers and their optimal designs for building vibration control. Eng. Struct. **21**(5), 454–463 (1999). https://doi.org/10.1016/S0141-0296(97)00213-7
4. Di Matteo, A., Lo Iacono, F., Navarra, G., Pirrotta, A.: Direct evaluation of the equivalent linear damping for TLCD systems in random vibration for pre-design purposes. Int. J. Nonlinear Mech. **63**(C), 19–30 (2014)
5. Di Matteo, A., Lo Iacono, F., Navarra, G., Pirrotta, A.: Experimental validation of a direct pre-design formula for TLCD. Eng. Struct. **75**(C), 528–538 (2014)
6. Di Matteo, A., Lo Iacono, F., Navarra, G., Pirrotta, A.: Innovative modeling of tuned liquid column damper motion. Commun. Nonlinear Sci. Numer. Simul. **23**(1–3), 229–244 (2015)
7. Di Matteo, A., Lo Iacono, F., Navarra, G., Pirrotta, A.: Optimal tuning of tuned liquid column damper systems in random vibration by means of an approximate formulation. Meccanica **50**(3), 795–808 (2015). https://doi.org/10.1007/s11012-014-0051-6
8. Di Matteo, A., Di Paola, M., Pirrotta, A.: Innovative modeling of tuned liquid column damper controlled structures. Smart Struct. Syst. **18**(1), 117–138 (2016)
9. Di Matteo, A., Lo Iacono, F., Navarra, G., Pirrotta, A.: The tlcd passive control: numerical investigations vs experimental results. In: ASME 2012 International Mechanical Engineering Congress and Exposition Dynamics, Control and Uncertainty, Parts A and B, vol. 4, pp. 1283–1290. ASME, New York (2012). https://doi.org/10.1115/IMECE2012-86568
10. FEMA P-695: Quantification of Building Seismic Performance Factors. Technical Representative, Federal Emergency Agency, Washington, D.C. (2009)
11. Fu, C., Ziegler, F.: Vibration prone multi-purpose buildings and towers effectively damped by tuned liquid column-gas dampers. Asian J. Civil Eng. **10**(1), 21–56 (2010)
12. Hochrainer, M.J., Ziegler, F.: Tuned liquid column gas damper in structural control: the salient features of a general purpose damping device and its application in buildings, bridges and dams. In: Lagaros, N.D. et al. (eds.) Design Optimization of Active and Passive Structural Control Systems, Chap. 7, pp. 150–179. Information Science Reference, Hershey, USA (2013)
13. Hochrainer, J.M.: Tuned liquid column damper for structural control. Acta Mech. **175**(1), 57–76 (2005). https://doi.org/10.1007/s00707-004-0193-z

14. Hochrainer, M.J., Ziegler, F.: Control of tall building vibrations by sealed tuned liquid column dampers. Struct. Control Health Monit. **13**(6), 980–1002 (2006). https://doi.org/10.1002/stc.90
15. Kareem, A.: Selected papers from the ninth international symposium on wind engineering modelling of base-isolated buildings with passive dampers under winds. J. Wind Eng. Ind. Aerodyn. **72**, 323–333 (1997). https://doi.org/10.1016/S0167-6105(97)00232-8
16. Kelly, J.M.: Aseismic base isolation: review and bibliography. Soil Dyn. Earthq. Eng. **5**(4), 202–216 (1986). https://doi.org/10.1016/0267-7261(86)90006-0
17. Kelly, J.M.: The role of damping in seismic isolation. Earthq. Eng. Struct. Dyn. **28**(1), 3–20 (1999). https://doi.org/10.1002/(SICI)1096-9845(199901)28:1<3::AID-EQE801>3.0.CO;2-D
18. Khalid, B., Ziegler, F.: A novel aseismic foundation system for multipurpose asymmetric buildings. Archive Appl. Mech. **82**(10), 1423–1437 (2012). https://doi.org/10.1007/s00419-012-0667-8
19. La Duc, V., Adam, C.: General on-off damping controller for semi-active tuned liquid column damper. J. Vib. Control (2016). https://doi.org/10.1177/1077546316648080
20. Love, J., Tait, M., Toopchi-Nezhad, H.: A hybrid structural control system using a tuned liquid damper to reduce the wind induced motion of a base isolated structure. Eng. Struct. **33**(3), 738–746 (2011). https://doi.org/10.1016/j.engstruct.2010.11.027
21. Palazzo, B., Betti, L.: Combined control strategies: base isolation and tuned mass damping. ISET J. Earthq. Technol. **36**, 121–137 (1999)
22. Palazzo, B., Petti, L.: Aspects of passive control of structural vibrations. Meccanica **32**(6), 529–544 (1997). https://doi.org/10.1023/A:1004244221103
23. Perez, R., Behdinan, K.: Particle swarm approach for structural design optimization. Comput. Struct. **85**(19–20), 1579–1588 (2007). https://doi.org/10.1016/j.compstruc.2006.10.013
24. Reiterer, M., Ziegler, F.: Bi-axial seismic activation of civil engineering structures equipped with tuned liquid column dampers. J. Seismol. Earthq. Eng. **6**(3), 45–60 (2004)
25. Reiterer, M., Ziegler, F.: Control of pedestrian-induced vibrations of long-span bridges. Struct. Control Health Monit. **13**(6), 1003–1027 (2006). https://doi.org/10.1002/stc.91
26. Roberts, J.B., Spanos, P.D.: Random Vibration and Statistical Linearization. Wiley, New York (1990)
27. Taniguchi, T., Kiureghian, A.D., Melkumyan, M.: Effect of tuned mass damper on displacement demand of base-isolated structures. Eng. Struct. **30**(12), 3478–3488 (2008). https://doi.org/10.1016/j.engstruct.2008.05.027
28. Tributsch, A., Adam, C.: Evaluation and analytical approximation of Tuned Mass Damper performance in an earthquake environment. Smart Structures and Systems **10**, 155–179 (2012)
29. Tsai, H.C.: The effect of tuned-mass dampers on the seismic response of base-isolated structures. Int. J. Solids Struct. **32**(8), 1195–1210 (1995). https://doi.org/10.1016/0020-7683(94)00150-U
30. Won, A.Y., Pires, J.A., Haroun, M.A.: Third international stochastic structural dynamics conference performance assessment of tuned liquid column dampers under random seismic loading. International Journal of Non-Linear Mechanics **32**(4), 745–758 (1997). https://doi.org/10.1016/S0020-7462(96)00118-7. http://www.sciencedirect.com/science/article/pii/S0020746296001187
31. Xiang, P., Nishitani, A.: Optimum design for more effective tuned mass damper system and its application to base-isolated buildings. Struct. Control Health Monit. **21**(1), 98–114 (2014). https://doi.org/10.1002/stc.1556
32. Yalla, S.K., Kareem, A.: Semiactive tuned liquid column dampers: experimental study. J. Struct. Eng. **129**(7), 960–971 (2003)
33. Yang, J.N., Danielians, A., Liu, S.C.: Aseismic hybrid control systems for building structures. J. Eng. Mech. **117**(4), 836–853 (1991)
34. Ziegler, F.: The tuned liquid column damper as a cost-effective alternative for the mechanical damper in civil engineering structures. J. Acoust. Vib. **12**, 25–39 (2007)
35. Ziegler, F.: Special design of tuned liquid column-gas dampers for the control of spatial structural vibrations. Acta Mech. **201**(1), 249–267 (2008). https://doi.org/10.1007/s00707-008-0062-2